



# Secondary Organic Aerosol Formation from the Oxidation of Decamethylcyclopentasiloxane at Atmospherically Relevant OH Concentrations

Sophia M. Charan<sup>1</sup>, Yuanlong Huang<sup>1</sup>, Reina S. Buenconsejo<sup>1</sup>, Qi Li<sup>2</sup>, David R. Cocker III<sup>2</sup>, and John H. Seinfeld<sup>1</sup>

<sup>1</sup>California Institute of Technology, Pasadena, California 91125, United States

<sup>2</sup>University of California – Riverside, Riverside, California 92521, United States

**Correspondence:** seinfeld@caltech.edu

**Abstract.** Decamethylcyclopentasiloxane (D5,  $C_{10}H_{30}O_5Si_5$ ) is measured at ppt levels outdoors and ppb levels indoors. Primarily used in personal care products, its outdoor concentration is correlated to population density. Since understanding the aerosol formation potential of volatile chemical products is critical to understanding particulate matter in urban areas, the secondary organic aerosol yield of D5 was studied under a range of OH concentrations, OH exposures,  $NO_x$  concentrations, and temperatures. The secondary organic aerosol (SOA) yield from the oxidation of D5 is extremely dependent on the OH concentration, and differing measurements of the SOA yield from the literature are resolved in this study. Here, we compare experimental results from environmental chambers and flow tube reactors. Generally, there are high SOA yields ( $> 68\%$ ) at OH mixing ratios of  $5 \times 10^9$  molec  $cm^{-3}$ . At atmospherically relevant OH concentrations, the SOA yield is largely  $< 5\%$  and usually  $\sim 1\%$ . This is significantly lower than SOA yields used in emission and particulate matter inventories and demonstrates the necessity of OH concentrations similar to the ambient environment when extrapolating SOA yield data to the outdoor atmosphere.

## 1 Introduction

Present in outdoor mixing ratios as high as  $\sim 40$  ppt, decamethylcyclopentasiloxane (D5,  $C_{10}H_{30}O_5Si_5$ ) has been observed in cities, rural areas, and the Arctic (Buser et al., 2013, 2014; Ahrens et al., 2014; McLachlan et al., 2010; Xu et al., 2019). D5 is used in personal care products, as well as for industrial purposes (Mackay et al., 2015); in 2004, over 17000 tons were used in the then European Union (Safron et al., 2015). Outdoor observations of D5 are population-dependent (Janecek et al., 2017; Gkatzelis et al., 2021) and this dependence is sufficiently reliable to be used as a tracer to differentiate the effects of population from that of motor vehicles (Coggon et al., 2018). The impact of D5 does not stop at population centers; its long atmospheric lifetime means that it is found in areas with low population densities.



Likely more than 90% of the D5 used is emitted into the atmosphere (Balducci et al., 2012; Hughes et al., 2012), though much of this may be first emitted indoors and only later exchanged to the outdoors: in an engineering classroom in the U.S. in 2014, ~30% by mass of the total volatile organic compounds (VOCs) were D5 (Tang et al., 2015). In an athletic center in the morning, D5 mixing ratios exceeded 6 ppb and emissions were attributed to the humans in the room (Finewax et al., 2020).  
25 Even the international space station was found to contain D5 (Carter et al., 2015).

Given the abundance of D5 in the ambient atmosphere, it is important to understand its fate. The major loss source of D5 is reaction with the hydroxyl radical; losses by reaction with  $\text{NO}_3$ ,  $\text{O}_3$ , and Cl are all negligible (Atkinson, 1991; Alton and Browne, 2020). The half-life of D5 outdoors is between 3.5 and 7 days, depending on the assumed global average OH concentration and the exact method used to calculate the reaction rate of OH with D5 (Safron et al., 2015; Xiao et al., 2015; Alton and Browne, 2020). Outside, both wet and dry deposition of D5 are negligible and methylsiloxanes do not photolyze in the actinic region (Hobson et al., 1997). Previous studies by Janecek et al. (2019) and Wu and Johnston (2017) measured secondary organic aerosol (SOA) yields, the ratios of the mass of organic aerosol formed to the mass of the precursor reacted, between 8 and 50%. This is a wide range and the conditions for these experiments were performed at OH concentrations much higher than those in the ambient atmosphere. By measuring the SOA formation potential of D5, we can better understand the  
35 contribution of volatile chemical products (VCPs) to aerosol levels in urban areas.

VCPs are a major (and perhaps majority) source of secondary organic aerosol in cities in the U.S., even urban areas that are not megacities (McDonald et al., 2018; Gkatzelis et al., 2021). Resolving uncertainties in the mass of SOA formed from VCPs is critical for refining SOA estimates and for creating policy to reduce SOA non-compliance in urban areas (Burkholder et al., 2017).

40 Researchers use both flow reactors and atmospheric chambers to measure the SOA yields of various compounds. While many results agree between the two methods of analysis, different reactors have varying benefits and operating conditions (e.g., OH concentrations, experiment length, precursor concentrations, humidity values). One must account for the particular attributes of the different reactors when extrapolating to the atmosphere.

## 2 Methods

45 Chamber experiments were performed in a temperature-controlled  $19 \text{ m}^3$  FEP Teflon Environmental Chamber run in batch mode. The chamber is hung in an enclosure, to reduce charge on the surface of the chamber, and is surrounded by ultraviolet lights centered at ~350 nm. Since the walls of the chamber are not rigid and data were collected continuously, the chamber decreased slightly in volume throughout the experiment, but never by more than 15%.

Prior to each chamber experiment, the contents of the chamber were flushed with air stripped of ozone, nitrogen oxides, water vapor, and organic carbon for > 24 h.  $\text{H}_2\text{O}_2$ , when used as an OH source, was injected by flowing air at 5 Lpm over liquid  $\text{H}_2\text{O}_2$  in a ~42°C water bath to obtain an  $[\text{H}_2\text{O}_2] \approx 2$  ppm. For the experiment that used methyl nitrite ( $\text{CH}_3\text{ONO}$ ), a glass bulb was evacuated and then filled to the desired pressure to obtain ~600 ppb in the chamber. After bringing the bulb



up to atmospheric pressure with nitrogen, it was flushed into the chamber with nitrogen. CH<sub>3</sub>ONO forms OH as described in Schwantes et al. (2019).

55 D5 (99%, TCI America) was injected into the chamber for Experiments 1–8 at room temperature by flowing nitrogen through a glass bulb at 5 Lpm for > 60 min. To obtain the desired initial surface area concentration, a sonicated, 0.06 M (0.15 M for Experiment 2) (NH<sub>4</sub>)<sub>2</sub>SO<sub>4</sub> solution was atomized to create aerosol that was then dried, passed through a TSI Model 3088 soft x-ray neutralizer, and injected into the chamber. For Experiment 7, no aerosol was injected. For Experiments 5–7, NO (506.9 ppm ± 2%, Airgas Specialty Gases, Certified Standard) was injected prior to the beginning of the experiment to achieve initial  
60 NO mixing ratios between 80 and 100 ppb. During Experiments 5 and 6, 1 ppb/min of NO was injected from the inception of radiation to the end of the experiment.

Experiments at higher OH mixing ratios were conducted in the Caltech Photooxidation Flow Tube (CPOT, Huang et al., 2017) at a constant flow rate of 4.88 Lpm and 23.0±0.1°C. The mean residence time of the CPOT was 671 ± 15 s and the diffusivity was 15 ± 2 cm<sup>2</sup> s<sup>-1</sup>, as calculated with a step injection of SO<sub>2</sub> using Equation 4 in Huang and Seinfeld (2019). For  
65 Experiments 9–15, clean air flowed through an ozone generator (UVP, 97-0067-01); for Experiments 16–19, O<sub>2</sub> flowed through the same generator to create higher concentrations of O<sub>3</sub>. The 254 nm lights photolyze O<sub>3</sub> to form O(<sup>1</sup>D), which reacts with H<sub>2</sub>O to form 2OH. After conditions were changed in the CPOT, no results were collected for at least 2 h. Data were averaged over between 1 and 11 h. D5 was injected through a syringe pump (Harvard Apparatus).

For all experiments, the concentration of D5 was measured with an HP 6890N gas chromatograph with a flame ionization  
70 detector (GC-FID) and a DB-5 column. Prior to the beginning of oxidation for the chamber experiments, all contents of the reactor were left to sit for 4 h (2.8 h for Experiment 7) and the initial concentration of D5 was taken as the mean concentration during this time. For the CPOT experiments, the initial concentration of D5 was calculated by measuring the outlet flow with lights off, no water source, and the absence of O<sub>3</sub>. For Experiment 9, the change in D5 was sufficiently small that it was within the uncertainty. For calculating the SOA yield for this experiment, we used the OH exposure calculated from the change in  
75 SO<sub>2</sub> concentration to find the change in D5 (7 ppb).

To calibrate the GC-FID, a small Teflon bag was filled with 35 ppm of D5 and later diluted to 9 ppm. This bag was sampled using the GC-FID and the concentration was verified with a Fourier transform infrared absorption (FT-IR) spectrometer with a 19 cm path length and absorption cross sections from the Pacific Northwest National Laboratory (PNNL) database. To minimize vapor-wall-loss to the FT-IR enclosure, multiple samples were taken until a consistent spectrum was achieved.

80 Gas-phase oxidation products were evaluated with a CF<sub>3</sub>O<sup>-</sup> chemical ionization mass spectrometer (CIMS) equipped with a Varian 1200 triple quadrupole mass analyzer. Concentrations of NO and NO<sub>2</sub> were measured with a Teledyne Nitrogen Oxide Analyzer (Model T200) and O<sub>3</sub> was found with a Horiba Ambient Monitor. Temperature and humidity were determined using a Vaisala HMM211 probe.

Aerosol volume was measured by a custom-built scanning mobility particle sizer (SMPS) with a 3081 TSI Differential  
85 Mobility Analyzer (DMA) and a TSI 3010 butanol condensation particle counter (CPC). The sheath flow rate was 2.64 Lpm and the aerosol flow rate from the chamber was 0.515 Lpm. A voltage scan from 15 to 9875 V was performed in 240 s every 330 s. Aerosol from the chamber flowed through an x-ray source to provide a known charge distribution, and the size distributions



were determined using the data inversion method described by Mai et al. (2018). Experiment 2 required a logarithmic fit to the largest particles present, as described in Charan et al. (2020), which is the source of the higher SOA yield uncertainty than in the other experiments (see Table 1). Conversions to mass concentration were performed by assuming that the aerosol density was  $1.1 \text{ g cm}^{-3}$ . This was estimated from data in Wu and Johnston (2017), which measured D5 secondary organic aerosol particles (using information in their Fig. S1a and Table S1).

Uncertainty estimates for all the instruments used in this study were determined as described in Charan et al. (2020). For the chamber experiments, particle-wall-deposition corrections were performed by calculating a diameter-independent first-order exponential fit ( $\beta = 1.7 \times 10^{-4} \text{ min}^{-1}$ ) to the particle volume concentration during the 3 h prior to the onset of oxidation and applying that correction to the rest of the experiment. This method was chosen because it aligns with a diameter-dependent fit as determined using the method in Charan et al. (2018) but is simpler and because, for the chamber experiments, minimal organic aerosol formed and so the particle diameters changed insignificantly throughout the duration of the experiment. For Experiment 7, in which no initial aerosol was present, no aerosol was generated throughout the experiment and so no correction was necessary to determine an apparent SOA yield of 0.

For the CPOT experiments, an upper estimate of the wall-deposition-corrected SOA mass was calculated with the inverse of the particle-size-dependent penetration efficiency of the flow-tube component of the reactor (data from Fig. 9d in Huang et al. 2017). Since particles nucleated in the CPOT, the penetration efficiency of only the flow-tube component (and not the static mixer prior to the region of reaction) was used. The penetration efficiency, however, is based on the entire flow tube and nucleated particles may not form immediately at the beginning of the flow-tube component; thus, the wall-deposition correction performed here is an upper bound of the correction. Note that this correction also neglects particle growth throughout the reactor and any particle-particle coagulation.

SOA yield ( $Y$ ) is defined by  $Y = \frac{\Delta \text{SOA}_{\text{corr}}}{\Delta \text{D5}}$ , where  $\Delta \text{SOA}_{\text{corr}}$  is the wall-deposition-corrected change in the aerosol mass concentration and  $\Delta \text{D5}$  is the mass concentration of reacted D5. Calculations were performed as described by Charan et al. (2020) and with the assumption that a particle, once deposited on the reactor wall, no longer acts as a condensation sink (Trump et al., 2016). Note that since so little aerosol was formed during the chamber experiments, this assumption had a negligible effect on the chamber results. For the CPOT experiments, any deviation from this assumption would have prevented the data from reaching steady-state.

While the vapor-wall-deposition lifetime of D5 to the chamber walls was estimated to be on the order of weeks, the propensity of vapor-wall-deposition of the oxidation products is not extensively investigated in this study. Even at high initial seed surface area concentrations, the SOA yield is still quite small (see Fig. S1). Alton and Browne (2020) estimated that, for their unseeded  $\sim 1 \text{ m}^3$  FEP Teflon chamber, 5% of the ester product of D5 oxidation might partition to the chamber walls during the reaction. The volume of the chamber used in this study is  $19 \text{ m}^3$  and seed aerosol is introduced prior to the experiment (except for Experiment 7, which was performed in the absence of seed aerosol). Even if 5% of the oxidation products were lost to the chamber walls, the SOA yields would still be within the reported uncertainty and sufficiently small so as not to affect any conclusions. The CPOT reactor is operated at steady-state and, therefore, any oxidation products that are in equilibrium with the bulk flow (i.e., not lost permanently to the quartz walls) do not need a vapor-wall-deposition correction.



For chamber experiments that employed  $\text{H}_2\text{O}_2$ , the OH concentration was calculated by fitting the gas-phase D5 concentration to a first-order exponential, fixing the initial point of the fit as the initial D5 concentration (fits had  $R^2 > 0.75$ ), and using the value for the reaction rate of OH with D5,  $k = 2.1 \pm 0.1 \times 10^{-12} \text{ cm}^3 \text{ molec}^{-1} \text{ s}^{-1}$ , which was measured using the relative rate method at  $297 \pm 3 \text{ K}$  (Alton and Browne, 2020). Note that other experimental evaluations of the reaction rate of OH with D5 that use the relative rates method vary by less than a factor of 2 (the reasons for this difference are not known), which would not affect the order of magnitude of the OH concentration estimate (Kim and Xu, 2017; Safron et al., 2015; Xiao et al., 2015). OH is the major loss source in the atmosphere and, we expect, in these experiments: losses to  $\text{O}_3$ ,  $\text{NO}_3$ , and Cl are all negligible (Atkinson, 1991; Alton and Browne, 2020). The ozone concentration did not affect the SOA yield results: Experiments 7 and 9, which were performed at substantially different  $\text{O}_3$  concentrations, still gave similar results for the SOA yield ( $0 \pm 0.1\%$  and  $0.8 \pm 0.8\%$  with an upper wall-deposition-corrected bound of 1.4%, respectively). For Experiment 8, in which  $\text{CH}_3\text{NO}_2$  served as the OH source, the sharp decrease in the D5 mixing ratio immediately after the commencement of radiation, followed by a gradual decrease in its concentration, indicates that two OH concentrations are relevant for this experiment. Since the D5 concentration is measured every  $\sim 21 \text{ min}$ , and the pulse with high OH concentrations occurs within the first 30 min of oxidation, the initial OH concentration is estimated with a two-point first-order exponential fit to the initial concentration and the first data point (12.3 min into radiation). The second OH concentration is estimated with a first-order exponential fit of the second point (33.3 min into radiation) to the end of the experiment.

OH exposure was calculated, for chamber experiments (Experiments 1–8) and experiments from Wu and Johnston (2017), as

$$[\text{OH}] * t = \frac{-1}{k_{\text{OH}+\text{D5}}} \ln \left( \frac{[\text{D5}]_{\text{end}}}{[\text{D5}]_0} \right), \quad (1)$$

where  $k_{\text{OH}+\text{D5}} = 2.1 \times 10^{-12} \text{ cm}^3 \text{ molec}^{-1} \text{ s}^{-1}$  (Alton and Browne, 2020). For the CPOT experiments (Experiments 9–19), OH exposure was calculated as

$$[\text{OH}] * t = \frac{-1}{k_{\text{OH}+\text{SO}_2}} \ln \left( \frac{[\text{SO}_2]_{\text{end}}}{[\text{SO}_2]_0} \right), \quad (2)$$

where  $k_{\text{OH}+\text{SO}_2} = 9 \times 10^{-13} \text{ cm}^3 \text{ molec}^{-1} \text{ s}^{-1}$  for an identical setup with  $\text{SO}_2$  instead of D5 (Janecek et al., 2019). The correlation between  $[\text{H}_2\text{O}]$  and OH exposure used to find the OH exposure for Experiments 9–19 is plotted in Fig. S2. Since the  $\text{O}_3$  concentrations differed in Experiments 9–15 and 16–19, the correlation between the  $[\text{H}_2\text{O}]$  and the OH exposure is also different. Note that, for Experiments 9–19, the OH exposure calculated using Equation 2 is about twice that calculated using Equation 1. This effect may be due to the regeneration of OH during the oxidation of D5 or the absorption of OH into the aerosol particles. Ideally, we seek to report the OH exposure excluding any regeneration. So, for Experiments 9–19, the OH exposure is calculated with Equation 2. Experiments 1–8 and those from Wu and Johnston (2017) use Equation 1, but have a positive uncertainty equal to their calculated OH exposure. Note that, for Experiments 1–8, OH concentration is calculated independently of the OH exposure. For Experiments 9–19, OH concentration is the ratio of the OH exposure to the residence time of the reactor.



### 155 3 Results

SOA yields and experimental conditions are given in Table 1 with estimated uncertainties. These SOA yields vary from 0 to 79% (114% at the upper bound of the wall-deposition-corrected value), an even wider range than that reported by the literature of 8–50% (Janecek et al., 2019; Wu and Johnston, 2017).

**Table 1.** Experimental conditions. All experiments began with  $[\text{NO}_2]_0 = 0$  ppb. The estimated uncertainty of  $[\text{NO}]_0$  is 5 ppb. Experiments in which NO was continuously injected maintained a rate of  $1 \text{ ppb min}^{-1}$ , starting at the inception of radiation. For Experiment 8, due to a pulse of OH when the  $\text{CH}_3\text{NO}_2$  initially photolyzes followed by a steadier concentration, two OH mixing ratios are given:  $[\text{OH}] = 2 \times 10^8 \text{ molec cm}^{-3}$  at the beginning of the experiment and  $[\text{OH}] = 1 \times 10^6 \text{ molec cm}^{-3}$  at its end. The uncertainties associated with the chamber and CPOT temperature are  $< 0.5^\circ\text{C}$  and  $0.1^\circ\text{C}$ , respectively. The uncertainty in the OH concentrations for the chamber and CPOT experiments are  $5 \times 10^5 \text{ molec cm}^{-3}$  and  $1 \times 10^6 \text{ molec cm}^{-3}$ , respectively. Uncertainties in the OH exposure for the CPOT experiments are  $5 \times 10^{10} \text{ molec s cm}^{-3}$ . For the chamber experiments, the uncertainties in the negative direction are  $4 \times 10^{10} \text{ molec cm}^{-3}$  and in the positive direction are the value of OH exposure reported for the experiment. For the CPOT experiments, the upper estimate of the wall-deposition-corrected SOA yield is shown in parentheses. The negative uncertainty in the SOA yields of the CPOT experiments is the reported uncertainty subtracted from the uncorrected Y and the positive uncertainty is the sum of the corrected Y and the reported uncertainty.

Label	Reactor	$[\text{NO}]_0$ (ppb)	Contin. NO Injection?	OH source	$[\text{OH}]$ ( $\text{molec cm}^{-3}$ )	$[\text{OH}]$ exposure ( $\text{molec s cm}^{-3}$ )	T ( $^\circ\text{C}$ )	$[\text{D5}]_0$ (ppb)	$[\text{Surf Area}]_0$ ( $10^3 \mu\text{m}^2 \text{ cm}^{-3}$ )	SOA Yield
1	Chamber	0	No	$\text{H}_2\text{O}_2$	$4.5 \times 10^6$	$9 \times 10^{10}$	26.6	$497 \pm 5$	$3.6 \pm 0.3$	$1.1 \pm 1.1\%$
2	Chamber	0	No	$\text{H}_2\text{O}_2$	$3.8 \times 10^6$	$8 \times 10^{10}$	26.5	$298 \pm 3$	$5.1 \pm 0.3$	$4.2 \pm 7\%$
3	Chamber	0	No	$\text{H}_2\text{O}_2$	$2.2 \times 10^6$	$6 \times 10^{10}$	27.6	$30 \pm 1$	$0.8 \pm 0.1$	$0 \pm 0.2\%$
4	Chamber	0	No	$\text{H}_2\text{O}_2$	$1.6 \times 10^6$	$3 \times 10^{10}$	17.7	$580 \pm 5$	$2.4 \pm 0.2$	$1.9 \pm 3\%$
5	Chamber	82	Yes	$\text{H}_2\text{O}_2$	$5.0 \times 10^6$	$1.3 \times 10^{11}$	26.6	$696 \pm 9$	$3.9 \pm 0.3$	$0.5 \pm 0.4\%$
6	Chamber	86	Yes	$\text{H}_2\text{O}_2$	$4.3 \times 10^6$	$9 \times 10^{10}$	26.6	$650 \pm 6$	$1.1 \pm 0.1$	$0.2 \pm 0.2\%$
7	Chamber	76	No	$\text{H}_2\text{O}_2$	$5.5 \times 10^6$	$1.3 \times 10^{11}$	23.6	$591 \pm 2$	0	$0 \pm 0.1\%$
8	Chamber	84	No	$\text{CH}_3\text{NO}_2$	$10^6 - 10^{8.3}$	$2.3 \times 10^{11}$	26.6	$603 \pm 5$	$0.6 \pm 0.1$	$0 \pm 0.1\%$
9	CPOT	0	No	$\text{O}_3$	$2.0 \times 10^7$	$1.4 \times 10^{10}$	23.0	$262 \pm 10$	0	$0.8(1.4) \pm 0.8\%$
10	CPOT	0	No	$\text{O}_3$	$2.3 \times 10^8$	$1.5 \times 10^{11}$	23.0	$262 \pm 10$	0	$1.3(2.1) \pm 0.1\%$
11	CPOT	0	No	$\text{O}_3$	$5.0 \times 10^8$	$3.3 \times 10^{11}$	23.0	$262 \pm 10$	0	$4.4(6.6) \pm 0.4\%$
12	CPOT	0	No	$\text{O}_3$	$2.3 \times 10^8$	$1.5 \times 10^{11}$	23.0	$262 \pm 10$	0	$3.3(4.8) \pm 0.3\%$
13	CPOT	0	No	$\text{O}_3$	$1.2 \times 10^9$	$7.8 \times 10^{11}$	23.0	$262 \pm 10$	0	$10.1(13.9) \pm 0.7\%$
14	CPOT	0	No	$\text{O}_3$	$1.5 \times 10^9$	$1.0 \times 10^{12}$	23.0	$262 \pm 10$	0	$17.1(23.5) \pm 1.2\%$
15	CPOT	0	No	$\text{O}_3$	$1.6 \times 10^9$	$1.1 \times 10^{12}$	23.0	$262 \pm 10$	0	$25.5(35.3) \pm 1.6\%$
16	CPOT	0	No	$\text{O}_3$	$4.7 \times 10^9$	$3.2 \times 10^{12}$	23.0	$246 \pm 3$	0	$79(114) \pm 5\%$
17	CPOT	0	No	$\text{O}_3$	$4.8 \times 10^9$	$3.2 \times 10^{12}$	23.0	$246 \pm 3$	0	$79(114) \pm 5\%$
18	CPOT	0	No	$\text{O}_3$	$4.7 \times 10^9$	$3.1 \times 10^{12}$	23.0	$82 \pm 3$	0	$73(100) \pm 5\%$
19	CPOT	0	No	$\text{O}_3$	$4.9 \times 10^9$	$3.3 \times 10^{12}$	23.0	$82 \pm 3$	0	$68(92) \pm 4\%$



Between the experiments performed here and those in the literature, the OH concentrations and OH exposures vary widely. Determining which of these is the relevant parameter is critical to extrapolating the SOA yield data to the atmosphere: environmentally relevant OH concentrations are on the order of  $10^6$  molec  $\text{cm}^{-3}$ , but since D5 is primarily lost to OH and has a half life of 3.5–7 days, OH exposures on the order of  $10^{12}$  molec s  $\text{cm}^{-3}$  are also relevant. Due to experimental limitations, in particular an inability to perform experiments for multiple days without diluting the sample and otherwise changing the conditions, these two variables are often correlated.

Nonetheless, differentiating the effects of these two variables is possible. If a chemical process occurs in which the reaction of D5 and OH forms an intermediate or a second-generation product that then either reacts with OH or fragments, then the competition between the two outcomes is moderated by the relative time required for self-reaction or reaction with OH. This means that, as the OH concentration increases, the OH-reaction product will predominate. If this is the chemistry that D5 undergoes, then we would expect the SOA yield to depend solely on the OH concentration and not on the OH exposure.

Figure 1a shows the relationship between the measured OH concentrations and SOA yields for the experiments performed here as well as those from the literature. There is very good agreement between the chamber and CPOT experiments for similar OH concentration (shown in purple and orange, respectively). Moreover, the sharp increase in measured Y starting at  $[\text{OH}] \approx 10^9$  molec  $\text{cm}^{-3}$  matches the hypothesis that there is a competitive process moderated by OH concentration.

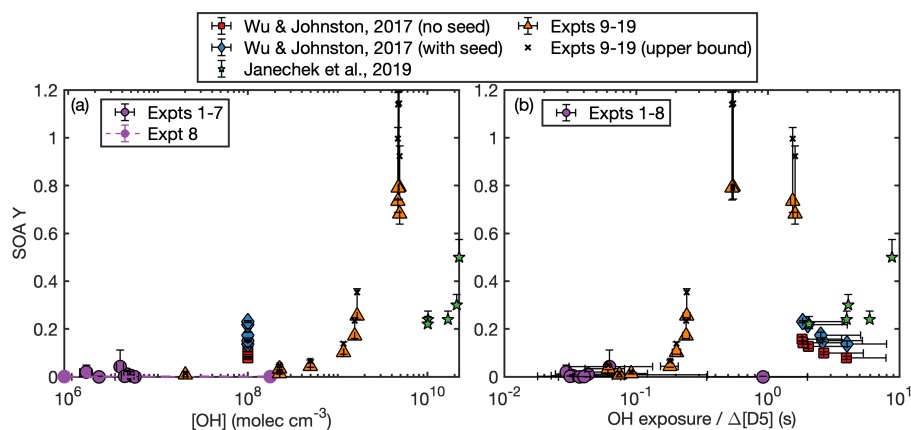


**Figure 1.** Measured SOA yield as a function of the (a) OH concentration and (b) OH exposure normalized to the amount of reacted D5 for the experiments performed here and by Janecek et al. (2019) and Wu and Johnston (2017). In panel (a), Experiment 8, which was performed with methyl nitrite, is shown in purple and not outlined in black and the initial and final OH concentrations are connected with a purple dashed line. The vast majority of this experiment was performed under the lower OH concentration.

Also plotted in Fig. 1a is the correlation between the  $[\text{OH}]$  and Y for experiments performed by Wu and Johnston (2017). These results, which were used by McDonald et al. (2018) for evaluating the contributions of D5 to aerosol levels in the Los Angeles Basin, were performed in a 50 L PFA photooxidation chamber with reported OH concentrations of  $\sim 10^8$  molec  $\text{cm}^{-3}$  (the error of which “was difficult to assess”) at  $27^\circ\text{C}$  and a relative humidity (RH) of 8–10%. Their data are neither vapor- nor wall-deposition corrected. For similar initial D5 concentrations (and, hence, for similar organic aerosol concentrations), the



measured SOA yields were uniformly higher in experiments that were initiated with ammonium sulfate seed than those that  
180 were not (see Fig. 3b). We, therefore, show the seeded and unseeded experiments in Fig. 1 in blue and red, respectively. OH  
concentration in the experiments reported by Wu and Johnston (2017) were calculated by replacing the precursor with SO<sub>2</sub>,  
measuring the formation of aerosol, and assuming that all the SO<sub>2</sub> reacts with OH to form H<sub>2</sub>SO<sub>4</sub> and all the sulfuric acid forms  
aerosol with minimal wall loss (Hall et al., 2013). Because of the uncertainties present for each step of this measurement, it  
seems reasonable that this [OH] estimate could be too low by at least a factor of 2.

185 Other instrumental and analysis uncertainties might close the gap between the OH concentrations measured by Wu and  
Johnston (2017) and the OH concentrations found in the experiments performed here. For example, the CPOT experiments and  
the Wu and Johnston (2017) experiments calculate the total OH exposure experienced in the flow reactor and then find the OH  
concentration by taking the ratio of this exposure and the residence time. Since the reactor used by Wu and Johnston (2017)  
is a rectangular bag, regions will exist with differing OH concentrations. If this reactor has slightly higher concentrations in  
190 some points or its residence time is overestimated or if the residence time for CPOT is a slight underestimate (we calculated an  
uncertainty of ~2%), this could account for the remaining disagreement between the data from the two experimental setups.

Furthermore, differences in the analysis could change the relevant SOA yields calculated. For Experiments 10–19, we mea-  
sured both the initial and the final D5 concentration and for Experiments 1–8 we continuously measured the concentration.  
Wu and Johnston (2017) measured the initial concentration and calculated the SOA yield by using the [OH] to estimate the  
195 amount of reacted D5. If Wu and Johnston (2017) underestimated the [OH], they might have correspondingly overestimated  
Y because they would have assumed less D5 reacted than in actuality. To achieve agreement to experiments performed here,  
then, the [OH] concentration could be different by less than a factor of 2 because of these confounding variables. We also  
assumed that the density of the SOA formed was 1.1 g cm<sup>-3</sup> and Wu and Johnston (2017) collected the aerosol onto filters  
and directly measured the mass formed. While we based our density estimate on, crudely, what was found in Wu and Johnston  
200 (2017) (particularly, their Experiments 1 and 5), the aerosol density in their experiments could have been as much as 1.6 g  
cm<sup>-3</sup>. Indeed, much secondary organic aerosol has a density of 1.4–1.6 g cm<sup>-3</sup>, which would account for a significant portion  
of the discrepancy (Kostenidou et al., 2007). Since the CPOT experiments were unseeded, seeded experiments increased the  
measured Y, which could also have led to better agreement.

Data from Janecek et al. (2019) show the opposite disagreement: OH concentrations are a factor of 2 too large to perfectly  
205 match the results presented here. Janecek et al. (2019) performed their experiments in a 13.3 L potential aerosol mass oxidation  
flow reactor (PAM OFR) with OH concentrations on the order of 10<sup>10</sup> molec cm<sup>-3</sup>. They reported the total OH exposure and  
calculated it similarly to the method used for CPOT (using Equation 2) and we convert this to the [OH] plotted by dividing  
this OH exposure by the residence time (calculated from the size of the reactor and the reported flow rate) and assuming that  
OH concentrations throughout the reactor are approximately constant. Just as with the CPOT experiments, their experiments  
210 are unseeded, and they measure the initial and final D5 concentration directly. They used an SOA density of 0.959 g cm<sup>-3</sup> to  
calculate Y and the positive error bars shown are an adjustment of their SOA yields to the 1.1 g cm<sup>-3</sup> used in the experiments  
performed here. While they corrected for particle loss downstream of their reactors, they did not account for those particles lost  
within their reactor; this could have led to an underestimate of their SOA yields. While the methods to calculate [OH] were





215 very similar, the CPOT and the PAM OFR are nevertheless different and, therefore, [OH] could vary locally in dissimilar ways between the reactors. Since the chemical mechanism shift would be based on the local OH concentration and not the average, a factor of 2 disagreement could be within the uncertainty. A comparison between predicted and estimated OH exposures for the PAM OFR indicates agreement only within a factor of 3 (Li et al., 2015; Janecek et al., 2019), so a factor of 2 disagreement in [OH] would seem to be with the uncertainties for the CPOT and the PAM OFR.

220 If the SOA yield depends on the OH exposure, instead of the OH concentration, we would expect that the dependence would actually be on the OH exposure normalized to the amount of reacted D5. That is, the number of OH radicals available per reacted D5 molecule, as is shown in Fig. 1b. This figure shows a factor of 10 disagreement between data from Wu and Johnston (2017) and Janecek et al. (2019) and that from the experiments conducted here. From the CPOT, Experiments 18 (OH exposure/ $\Delta$ [D5]=1.5 s, Y=73%) and 19 (OH exposure/ $\Delta$ [D5]=1.6 s, Y=68%), which had [D5]<sub>0</sub>=82 ppb, differ significantly from Experiments 16 and 17 (OH exposure/ $\Delta$ [D5]=0.5 s, Y=79%), which had [D5]<sub>0</sub>=246 ppb and otherwise identical 225 experimental conditions. This suggests that OH exposure is not the driving force in determining the SOA yield.

The major difference in Experiments 16–17 and 18–19 is the percent of D5 that reacted by the end of the experiment: 97% for Experiment 16, 98% for Experiment 17, and 100% for Experiments 18–19. Figure 2 shows the fraction reacted compared to the SOA yield for experiments performed in this study and those in the literature. This fit could indicate that there are later generation oxidation products that form large amounts of aerosol and that the gas-phase reaction rate to form the low-volatility 230 later-generation oxidation product is slower than the gas-phase reaction rate to form the first-generation product (Kroll and Seinfeld, 2008). However, if this were the case, Experiments 18–19 (Y=73% and 68%), in which all of the initial D5 reacted throughout the experiment, should show higher SOA yields than Experiments 16–17 (Y=79%), which they do not. Additionally, if later generation oxidation products produced more aerosol, there should be a correlation between Y and the OH exposure normalized to the amount of reacted D5 (Fig. 1b), which is also not accurate. The color axis in Fig. 2 indicates that across 235 studies the fraction of D5 reacted correlates with the [OH]. So, there is no reason to suspect that it is the later-generation products that matter instead of the OH concentration for determining SOA yield.

If OH concentration is the strict determinant of the SOA yield, Experiments 16–17 should give the same SOA yields as Experiments 18–19. These experiments do have similar SOA yields, and Experiments 16–18 are all within error. If there is a difference, it might be attributed to a dependence on the organic aerosol mass concentration (M) at high [OH]. This would 240 indicate that at high mass loadings, relatively more low-volatility products partition into the particle phase. This could also explain the disagreement in Fig. 1a between the CPOT experiments and the data from Janecek et al. (2019). Partitioning between the particle and gas phases does not significantly change the dependence of Y on [OH] for the experiments performed in this study: as shown in Fig. 3a, Experiment 15 (triangle with M=717  $\mu\text{g m}^{-3}$ ) has a similar M as Experiments 18 and 19 (triangles with M of 917 and 851  $\mu\text{g m}^{-3}$ , respectively) but due to their differing [OH], they have very different SOA yields. 245 Fig. 3b shows the same for a comparison between the lower [OH] experiments (Experiments 1–10); even at the same M, the OH concentration is what matters for determining Y. Note that the seed-surface-area dependence of experiments performed by Wu and Johnston (2017) is likely a result of the loss of oxidation product to the reactor's walls instead of to condensation onto particles suspended in the bulk of the chamber. The vast majority of the experiments performed under atmospherically relevant

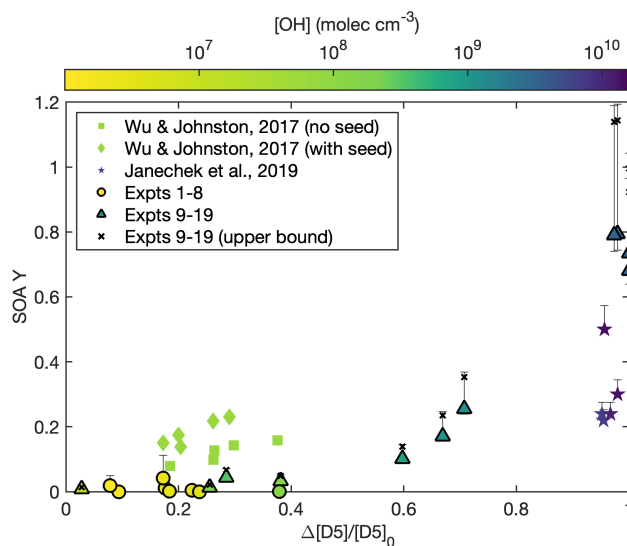


**Figure 2.** Measured SOA yield as a function of the fraction of D5 reacted at the end of the experiment. The color of each point indicates the OH concentration for the experiment. Experiments performed here are circles and triangles and are outlined in black, those by Janecek et al. (2019) are stars, and those by Wu and Johnston (2017) are squares and diamonds. The wall-deposition-corrected data for Experiments 9–19 are shown as black Xs.

OH concentrations were also seeded and showed low SOA yields. For all experiments with  $[OH] < 10^8$  molec  $\text{cm}^{-3}$ , the SOA yield is still  $< 5\%$  and, in general, is closer to  $\sim 1\%$ .

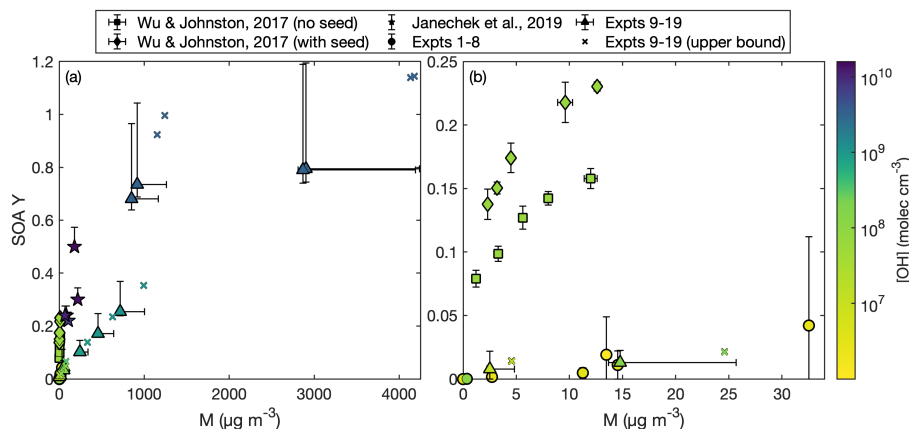


**Figure 3.** SOA yield as a function of organic aerosol mass concentration ( $M$ ) as compared to that reported by Wu and Johnston (2017) and Janecek et al. (2019). The color axis is the OH concentration. Even for similar  $M$ , an order of magnitude discrepancy exists in SOA yield. Panel (a) shows the entire scale and panel (b) focuses on experiments with  $M < 34 \mu\text{g m}^{-3}$ . Since the experiments reported by Wu and Johnston (2017) showed a dependence on the presence or absence of aerosol seed, those experiments are shown separately. CPOT experiments performed in this study were conducted without seed aerosol.



We do not expect that either relative humidity or temperature affect the SOA yield sufficiently that these would account for the vastly different measured SOA yields under different OH concentration. Experiments 1–8 were performed at RH levels between 2 and 6%, Experiments 9–19 were between 0 and 30% RH, those by Wu and Johnston (2017) were performed at 27°C and a RH of 8–10%, and the experiments from Janecek et al. (2019) were run at 24°C and an RH of 25% or 45%. At  
255 similar values of relative humidity but different OH concentrations (e.g., Experiments 9–12, which all have  $\text{RH} \leq 6\%$ ), the OH concentration matters for determining the SOA yield. For Experiments 3 and 4, the lowest and highest temperatures studied here (17.7 and 27.6°C, respectively), the measured SOA Y varies by  $< 2\%$ , which is within the uncertainty.

The  $\text{NO}_x$  concentrations also do not seem to affect the SOA yield, as discussed in Appendix A. While the D5 oxidation chemistry may depend on the NO mixing ratio (but not on the  $\text{NO}_2$  mixing ratio), this has no effect on the measured SOA  
260 yield.

#### 4 Conclusions

The atmospheric aerosol formation potential of D5 was investigated under a range of OH concentrations and exposures. While secondary organic aerosol (SOA) yields can reach 79% (114% at the upper limit) at OH mixing ratios of  $\sim 5 \times 10^9 \text{ molec cm}^{-3}$ , at atmospherically relevant OH concentrations ( $[\text{OH}] \lesssim 10^{7.5} \text{ molec cm}^{-3}$ ), SOA yields do not exceed 5% and are likely  $\sim 1\%$ .  
265 It is the OH concentration, and not the OH exposure, that affects the SOA yield.

This demonstrates the importance of extrapolating to the atmosphere at OH concentrations close to atmospheric levels and of using the appropriate reactor for the chemistry of a precursor to determine the secondary organic aerosol formation: if OH concentration is dominant, environmental chambers may be more useful, but if OH exposure matters, then flow tubes that have high OH mixing ratios may be the best tool.

270 Despite the relatively low SOA yields of D5 measured here at ambient OH concentrations, silicon has been observed in ambient aerosol and its concentration is likely somewhat population (and not vehicle) dependent (Bzdek et al., 2014; Pennington et al., 2012). Since D5 is so abundant, it could be possible that the silicon present is from D5 or other volatile methyl siloxanes, just in lower concentrations than expected. Another possibility is that silicon in the aerosol-phase comes from polydimethylsiloxanes (Weschler, 1988).

275 Since the aerosol formed from volatile chemical products (VCPs) may dominate the high concentrations of particulate matter found in urban areas (McDonald et al., 2018), understanding those VCPs that have high aerosol-formation potential and those which do not is important for formulating policy to reduce human exposure to organic aerosol.

#### Appendix A: $\text{NO}_x$ -Dependence of SOA Yield

For atmospherically relevant OH concentrations, the SOA yield does not change depending on the  $\text{NO}_x$  concentration: experi-  
280 ments with no  $\text{NO}_x$  present are on both the lower and higher end of the SOA yields for the chamber experiments. Those with a continuous injection of NO throughout the experiment, which ensured that the  $\text{NO}/\text{HO}_2$  ratio remained high even as the NO



reacted, had SOA yields similar to both the no  $\text{NO}_x$  and the initial NO experiments. This indicates that different NO mixing ratios did not have an effect on the measured SOA yield.

This does not imply that the chemistry is independent of NO concentration. Indeed, the concentrations of gas-phase fragments detected by the CIMS at  $m/z$  139, 169, 243, and 317, which likely correspond to oxygenated fragments of D5, depend on the NO concentration but not the  $\text{NO}_2$  concentration. Figure A1 shows the signal for these fragments normalized to the reagent ion as a function of the NO concentration at any time. Note that, since some of the methyl nitrite is detected as NO, data from Experiment 8 were not included. Figure A2 shows the NO and  $\text{NO}_2$  concentrations in each experiment as a function of time.

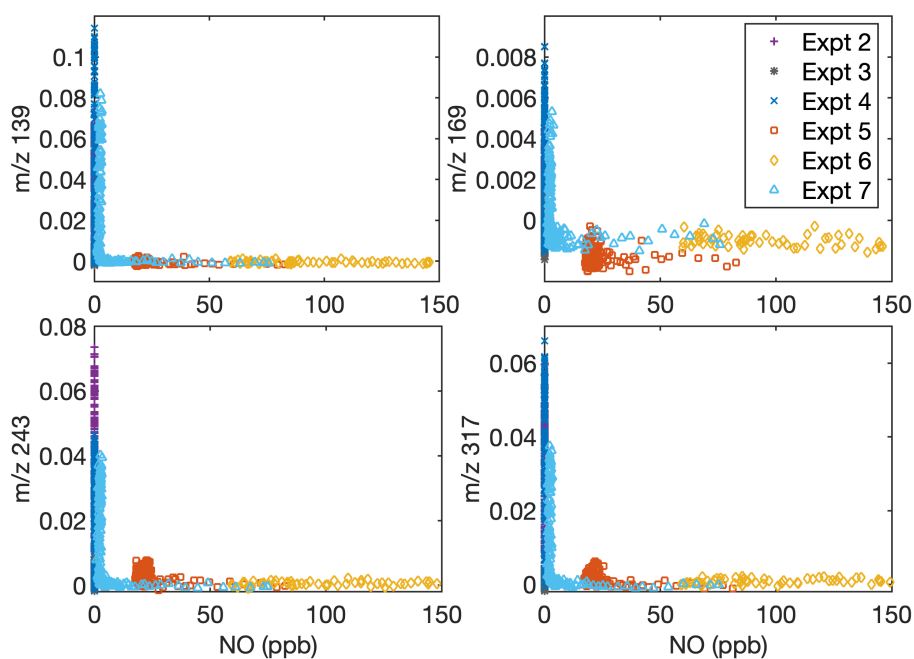


**Figure A1.** Dependence of gas-phase D5 oxidation products on the NO concentration in the chamber indicates that oxidation chemistry changes depending on NO concentrations. Signals normalized to the reagent concentrations with (a)  $m/z=139$ , (b)  $m/z=169$ , (c)  $m/z=243$ , and (d)  $m/z=317$  are shown as a function of NO concentration. Experiment 6 has  $[\text{NO}]$  extending to  $>450$  ppb, but since the normalized signal remains close to 0, data above  $[\text{NO}]=150$  ppb are cut off for clarity. Because of the inaccuracy of NO measurements during oxidation when methyl nitrite is present, Experiment 8 is not included.

Fu et al. (2020) found that the gas-phase rearrangement of methylsiloxanes is dependent on the  $\text{NO}/\text{HO}_2$  ratio. A comparison of Figs. A1 and A3 shows that the concentration of some gas-phase fragments is dependent on the NO mixing ratio but not on the  $\text{NO}_2$  mixing ratio. This is consistent with gas-phase products depending on the  $\text{NO}/\text{HO}_2$  ratio. Note that at all  $\text{NO}/\text{HO}_2$  ratios investigated, aerosol formation is still minimal when  $[\text{OH}]$  is small.

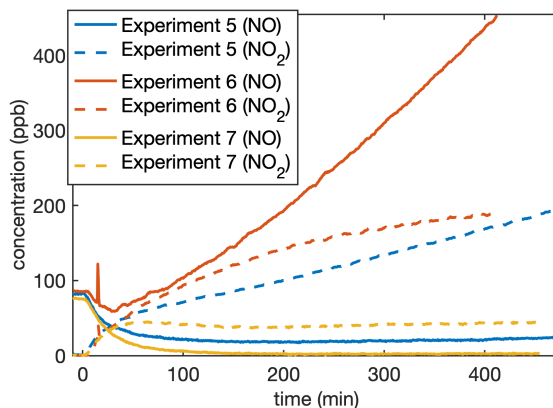


**Figure A2.** For the experiments that included  $\text{NO}_x$ , the NO and  $\text{NO}_2$  concentrations as a function of the time since the onset of oxidation. Experiment 8 is not included, since methyl nitrite was present. The measurement uncertainty is  $\sim 5$  ppb, but any organonitrates would also be measured as  $\text{NO}_2$ .

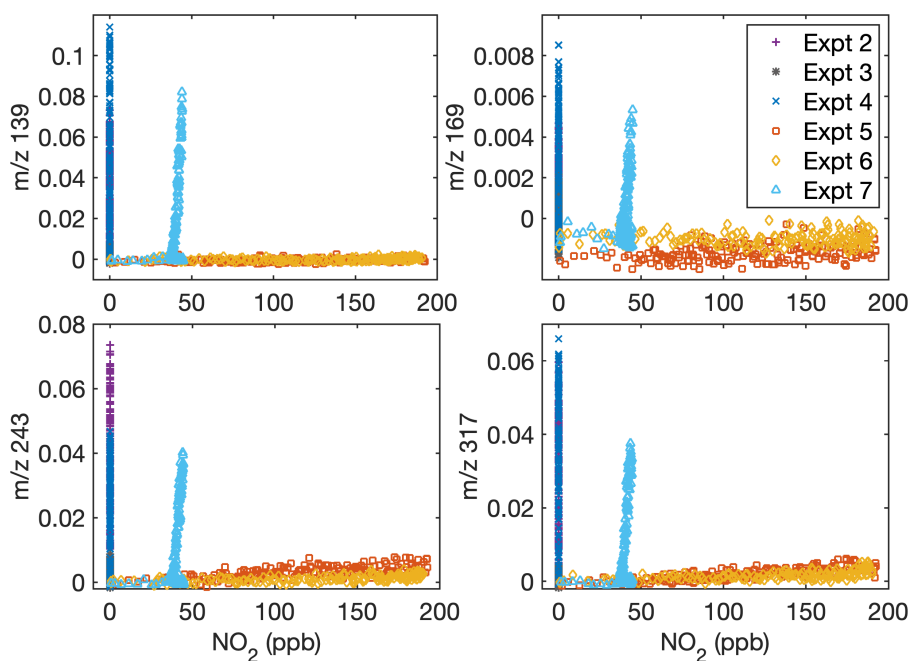


**Figure A3.** Dependence of gas-phase D5 oxidation products on the  $\text{NO}_2$  concentration in the chamber indicates that oxidation chemistry does not depend on  $\text{NO}_2$  (but does depend on NO, see Fig. A1). Signals normalized to the reagent concentrations with (a)  $m/z=139$ , (b)  $m/z=169$ , (c)  $m/z=243$ , and (d)  $m/z=317$  are shown as a function of  $\text{NO}_2$  concentration. Because of the inaccuracy of  $\text{NO}_2$  measurements during oxidation when methyl nitrite is present, Experiment 8 is not included.



*Data availability.* Chamber data available upon request and through the Index of Chamber Atmospheric Research in the United States (ICARUS).

295 *Author contributions.* SMC designed the experiments, carried out the data collection and analysis, and wrote the manuscript. YH assisted with the CPOT experiments. RSB and QL participated in discussions about the study. DRC secured funding for the project. JHS supervised the work. All authors reviewed and edited the manuscript.

*Competing interests.* The authors declare that they have no conflict of interest.

300 *Acknowledgements.* The authors would like to thank Nathan Dalleska for his assistance with the GC-FID; John Crouse for his general help and for synthesis of  $\text{CF}_3\text{O}^-$  for the CIMS; Paul Wennberg for the use of his FT-IR and for his insight during discussions of the system; Lu Xu and Benjamin Schulze for useful input; and Mitchell Alton and Eleanor Browne for helpful discussions. The project was funded by the California Air Resources Board (Contract #18RD009). SMC and RSB were funded by the National Science Foundation Graduate Research Fellowship program (#1745301).



## References

- 305 Ahrens, L., Harner, T., and Shoeib, M.: Temporal Variations of Cyclic and Linear Volatile Methylsiloxanes in the Atmosphere Using Passive Samplers and High-Volume Air Samplers, *Environ. Sci. Technol.*, 48, 9374–9381, <https://doi.org/10.1021/es502081j>, 2014.
- Alton, M. W. and Browne, E. C.: Atmospheric Chemistry of Volatile Methyl Siloxanes: Kinetics and Products of Oxidation by OH Radicals and Cl Atoms, *Environ. Sci. Technol.*, 54, 5992–5999, <https://doi.org/10.1021/acs.est.0c01368>, 2020.
- Atkinson, R.: Kinetics of the Gas-Phase Reactions of a Series of Organosilicon Compounds with OH and NO<sub>3</sub> Radicals and O<sub>3</sub> at 297 ± 2  
310 K, *Environ. Sci. Technol.*, 25, 863–866, <https://doi.org/10.1021/es00017a005>, 1991.
- Balducci, C., Perilli, M., Romagnoli, P., and Cecinato, A.: New Developments on Emerging Organic Pollutants in the Atmosphere, *Environ. Sci. Pollut. R.*, 19, 1875–1884, <https://doi.org/10.1007/s11356-012-0815-2>, 2012.
- Burkholder, J. B., Abbatt, J. P., Barnes, I., Roberts, J. M., Melamed, M. L., Ammann, M., Bertram, A. K., Cappa, C. D., Carlton, A. M. G., Carpenter, L. J., Crowley, J. N., Dubowski, Y., George, C., Heard, D. E., Herrmann, H., Keutsch, F. N., Kroll, J. H., McNeill, V. F., Ng,  
315 N. L., Nizkorodov, S. A., Orlando, J. J., Percival, C. J., Picquet-Varrault, B., Rudich, Y., Seakins, P. W., Surratt, J. D., Tanimoto, H., Thornton, J. A., Zhu, T., Tyndall, G. S., Wahner, A., Weschler, C. J., Wilson, K. R., and Ziemann, P. J.: The Essential Role for Laboratory Studies in Atmospheric Chemistry, *Environ. Sci. Technol.*, pp. 2519–2528, <https://doi.org/10.1021/acs.est.6b04947>, 2017.
- Buser, A. M., Kierkegaard, A., Bogdal, C., MacLeod, M., Scheringer, M., and Hungerbühler, K.: Concentrations in Ambient Air and Emissions of Cyclic Volatile Methylsiloxanes in Zurich, Switzerland, *Environ. Sci. Technol.*, 47, 7045–7051,  
320 <https://doi.org/10.1021/es3046586>, 2013.
- Buser, A. M., Bogdal, C., MacLeod, M., and Scheringer, M.: Emissions of Decamethylcyclopentasiloxane from Chicago, *Chemosphere*, 107, 473–475, <https://doi.org/10.1016/j.chemosphere.2013.12.034>, 2014.
- Bzdek, B. R., Horan, A. J., Pennington, M. R., Janecek, N. J., Baek, J., Stanier, C. O., and Johnston, M. V.: Silicon is a Frequent Component of Atmospheric Nanoparticles, *Environ. Sci. Technol.*, 48, 11 137–11 145, <https://doi.org/10.1021/es5026933>, 2014.
- 325 Carter, L., Perry, J., Kayatin, M. J., Wilson, M., Gentry, G. J., Bowman, E., Monje, O., Rector, T., and Steele, J.: Process Development for Removal of Siloxanes from ISS Atmosphere, in: 45th International Conference on Environmental Systems (July 12–16, 2015), 74, Bellevue, Washington, <http://hdl.handle.net/2346/64361>, 2015.
- Charan, S. M., Kong, W., Flagan, R. C., and Seinfeld, J. H.: Effect of Particle Charge on Aerosol Dynamics in Teflon Environmental Chambers, *Aerosol Sci. Technol.*, 52, 854–871, <https://doi.org/10.1080/02786826.2018.1474167>, 2018.
- 330 Charan, S. M., Buenconsejo, R. S., and Seinfeld, J. H.: Secondary Organic Aerosol Yields from the Oxidation of Benzyl Alcohol, *Atmos. Chem. Phys.*, 20, 13 167–13 190, <https://doi.org/10.5194/acp-20-13167-2020>, 2020.
- Coggon, M. M., McDonald, B. C., Vlasenko, A., Veres, P. R., Bernard, F., Koss, A. R., Yuan, B., Gilman, J. B., Peischl, J., Aikin, K. C., Durant, J., Warneke, C., Li, S. M., and De Gouw, J. A.: Diurnal Variability and Emission Pattern of Decamethylcyclopentasiloxane (D5) from the Application of Personal Care Products in Two North American Cities, *Environ. Sci. Technol.*, 52, 5610–5618,  
335 <https://doi.org/10.1021/acs.est.8b00506>, 2018.
- Finewax, Z., Pagonis, D., Claffin, M. S., Handschy, A. V., Brown, W. L., Jenks, O., Nault, B. A., Day, D. A., Lerner, B. M., Jimenez, J. L., Ziemann, P. J., and de Gouw, J. A.: Quantification and Source Characterization of Volatile Organic Compounds from Exercising and Application of Chlorine-Based Cleaning Products in a University Athletic Center, *Indoor Air*, pp. 1–17, <https://doi.org/10.1111/ina.12781>, 2020.



- 340 Fu, Z., Xie, H. B., Elm, J., Guo, X., Fu, Z., Fu, Z., and Chen, J.: Formation of Low-Volatile Products and Unexpected High Formaldehyde Yield from the Atmospheric Oxidation of Methylsiloxanes, *Environ. Sci. Technol.*, **54**, 7136–7145, <https://doi.org/10.1021/acs.est.0c01090>, 2020.
- Gkatzelis, G. I., Coggon, M. M., McDonald, B. C., Peischl, J., Aikin, K. C., Gilman, J. B., Trainer, M., and Warneke, C.: Identifying Volatile Chemical Product Tracer Compounds in U.S. Cities, *Environ. Sci. Technol.*, **55**, 188–199, <https://doi.org/10.1021/acs.est.0c05467>, 2021.
- 345 Hall, W. A., Pennington, M. R., and Johnston, M. V.: Molecular Transformations Accompanying the Aging of Laboratory Secondary Organic Aerosol, *Environ. Sci. Technol.*, **47**, 2230–2237, <https://doi.org/10.1021/es303891q>, 2013.
- Hobson, J. F., Atkinson, R., and L, C. W. P.: Chapter 6: Volatile Methylsiloxanes, in: *The Handbook of Environmental Chemistry Vol. 3 Part H: Organosilicon Materials*, edited by Chandra, G., 9, pp. 137–180, Springer, Berlin, <https://doi.org/10.1007/978-3-540-68331-5>, 1997.
- Huang, Y. and Seinfeld, J. H.: A Note on Flow Behavior in Axially-Dispersed Plug Flow Reactors with Step Input of Tracer, *Atmos. Environ.*
- 350 X, **1**, 1–6, <https://doi.org/10.1016/j.aeaoa.2019.100006>, 2019.
- Huang, Y., Coggon, M. M., Zhao, R., Lignell, H., Bauer, M. U., Flagan, R. C., and Seinfeld, J. H.: The Caltech Photooxidation Flow Tube reactor: Design, Fluid Dynamics and Characterization, *Atmos. Meas. Tech.*, **10**, 839–867, <https://doi.org/10.5194/amt-10-839-2017>, 2017.
- Hughes, L., Mackay, D., Powell, D. E., and Kim, J.: An Updated State of the Science EQC Model for Evaluating Chemical Fate in the Environment: Application to D5 (Decamethylcyclopentasiloxane), *Chemosphere*, **87**, 118–124, <https://doi.org/10.1016/j.chemosphere.2011.11.072>, 2012.
- 355 Janecek, N. J., Hansen, K. M., and Stanier, C. O.: Comprehensive Atmospheric Modeling of Reactive Cyclic Siloxanes and Their Oxidation Products, *Atmos. Chem. Phys.*, **17**, 8357–8370, <https://doi.org/10.5194/acp-17-8357-2017>, 2017.
- Janecek, N. J., Marek, R. F., Bryngelson, N., Singh, A., Bullard, R. L., Brune, W. H., and Stanier, C. O.: Physical Properties of Secondary Photochemical Aerosol from OH Oxidation of a Cyclic Siloxane, *Atmos. Chem. Phys.*, **19**, 1649–1664, [https://doi.org/10.5194/acp-19-](https://doi.org/10.5194/acp-19-1649-2019)
- 360 [1649-2019](https://doi.org/10.5194/acp-19-1649-2019), 2019.
- Kim, J. and Xu, S.: Quantitative Structure-Reactivity Relationships of Hydroxyl Radical Rate Constants for Linear and Cyclic Volatile Methylsiloxanes, *Environ. Toxicol. Chem.*, **36**, 3240–3245, <https://doi.org/10.1002/etc.3914>, 2017.
- Kostenidou, E., Pandis, S. N., Pathak, R. K., Pandis, S. N., Kostenidou, E., and Pandis, S. N.: An Algorithm for the Calculation of Secondary Organic Aerosol Density Combining AMS and SMPS Data, *Aerosol Sci. Technol.*, **41**, 1002–1010, <https://doi.org/10.1080/02786820701666270>, 2007.
- 365 Kroll, J. H. and Seinfeld, J. H.: Chemistry of Secondary Organic Aerosol: Formation and Evolution of Low-Volatility Organics in the Atmosphere, *Atmos. Environ.*, **42**, 3593–3624, <https://doi.org/10.1016/j.atmosenv.2008.01.003>, 2008.
- Li, R., Palm, B. B., Ortega, A. M., Hlywiak, J., Hu, W., Peng, Z., Day, D. A., Knote, C., Brune, W. H., Gouw, J. A. D., and Jimenez, J. L.: Modeling the Radical Chemistry in an Oxidation Flow Reactor: Radical Formation and Recycling, Sensitivities, and the OH Exposure
- 370 Estimation Equation, *J. Phys. Chem. A*, **119**, 4418–4432, <https://doi.org/10.1021/jp509534k>, 2015.
- Mackay, D., Cowan-Ellsberry, C. E., Powell, D. E., Woodburn, K. B., Xu, S., Kozerski, G. E., and Kim, J.: Decamethylcyclopentasiloxane (D5) Environmental Sources, Fate, Transport, and Routes of Exposure, *Environ. Toxicol. Chem.*, **34**, 2689–2702, <https://doi.org/10.1002/etc.2941>, 2015.
- Mai, H., Kong, W., Seinfeld, J. H., and Flagan, R. C.: Scanning DMA Data Analysis II. Integrated DMA-CPC Instrument Response and Data
- 375 Inversion, *Aerosol Sci. Technol.*, **6826**, 1–35, <https://doi.org/10.1080/02786826.2018.1528006>, 2018.
- McDonald, B. C., de Gouw, J. A., Gilman, J. B., Jathar, S. H., Akherati, A., Cappa, C. D., Jimenez, J. L., Lee-Taylor, J., Hayes, P. L., McKeen, S. A., Cui, Y. Y., Kim, S.-W., Gentner, D. R., Isaacman-VanWertz, G., Goldstein, A. H., Harley, R. A., Frost, G. J., Roberts, J. M., Ryerson,





- T. B., and Trainer, M.: Volatile Chemical Products Emerging as Largest Petrochemical Source of Urban Organic Emissions, *Science*, 359, 760–764, <https://doi.org/10.1126/science.aaq0524>, 2018.
- 380 McLachlan, M. S., Kierkegaard, A., Hansen, K. M., Van Egmond, R., Christensen, J. H., and Skjøth, C. A.: Concentrations and Fate of Decamethylcyclotrisiloxane (D5) in the Atmosphere, *Environ. Sci. Technol.*, 44, 5365–5370, <https://doi.org/10.1021/es100411w>, 2010.
- Pennington, M. R., Klems, J. P., Bzdek, B. R., and Johnston, M. V.: Nanoparticle Chemical Composition and Diurnal Dependence at the CalNex Los Angeles Ground Site, *J. Geophys. Res.-Atmos.*, 117, 1–9, <https://doi.org/10.1029/2011JD017061>, 2012.
- Safron, A., Strandell, M., Kierkegaard, A., and Macleod, M.: Rate Constants and Activation Energies for Gas-Phase Reactions of Three  
385 Cyclic Volatile Methyl Siloxanes with the Hydroxyl Radical, *Int. J. Chem. Kinet.*, 47, 420–428, <https://doi.org/10.1002/kin.20919>, 2015.
- Schwantes, R. H., Charan, S. M., Bates, K. H., Huang, Y., Nguyen, T. B., Mai, H., Kong, W., Flagan, R. C., and Seinfeld, J. H.: Low-Volatility Compounds Contribute Significantly to Isoprene Secondary Organic Aerosol (SOA) under high-NO<sub>x</sub> Conditions, *Atmos. Chem. Phys.*, 19, 7255–7278, <https://doi.org/10.5194/acp-19-7255-2019>, 2019.
- Tang, X., Misztal, P. K., Nazaroff, W. W., and Goldstein, A. H.: Siloxanes are the Most Abundant Volatile Organic Compound Emitted from  
390 Engineering Students in a Classroom, *Environ. Sci. Technol. Lett.*, 2, 303–307, <https://doi.org/10.1021/acs.estlett.5b00256>, 2015.
- Trump, E. R., Epstein, S. A., Riipinen, I., and Donahue, N. M.: Wall Effects in Smog Chamber Experiments: A Model Study, *Aerosol Sci. Technol.*, 50, 1180–1200, <https://doi.org/10.1080/02786826.2016.1232858>, 2016.
- Weschler, C. J.: Polydimethylsiloxanes Associated with Indoor and Outdoor Airborne Particles, *Sci. Total Environ.*, 73, 53–63, [https://doi.org/10.1016/0048-9697\(88\)90186-6](https://doi.org/10.1016/0048-9697(88)90186-6), 1988.
- 395 Wu, Y. and Johnston, M. V.: Aerosol Formation from OH Oxidation of the Volatile Cyclic Methyl Siloxane (cVMS) Decamethylcyclotrisiloxane, *Environ. Sci. Technol.*, 51, 4445–4451, <https://doi.org/10.1021/acs.est.7b00655>, 2017.
- Xiao, R., Zammit, I., Wei, Z., Hu, W. P., MacLeod, M., and Spinney, R.: Kinetics and Mechanism of the Oxidation of Cyclic Methylsiloxanes by Hydroxyl Radical in the Gas Phase: An Experimental and Theoretical Study, *Environ. Sci. Technol.*, 49, 13322–13330, <https://doi.org/10.1021/acs.est.5b03744>, 2015.
- 400 Xu, S., Warner, N., Bohlin-Nizzetto, P., Durham, J., and McNett, D.: Long-Range Transport Potential and Atmospheric Persistence of Cyclic Volatile Methylsiloxanes Based on Global Measurements, *Chemosphere*, 228, 460–468, <https://doi.org/10.1016/j.chemosphere.2019.04.130>, 2019.